Management and Production Engineering Review
Volume 9 • Number 4 • December 2018 • pp. 56–69
DOI: 10.24425/119546

ANALYSIS OF THROUGH TRANSMISSION LASER WELDING OF NYLON6 BY FINITE ELEMENT SIMULATION

Santosh Kumar Gupta[1], Pradip Kumar Pal[2]

[1] *Jadavpur University*
[2] *Jadavpur University, Mechanical Engineering Department*

Corresponding author:
Santosh Kumar Gupta
Jadavpur University
Kolkata, India
phone: 9337099888
e-mail: santoshduce@gmail.com

Received: 30 August 2017
Accepted: 5 September 2018

Abstract
Over the years laser welding has evolved as a fabrication process capable of overcoming the limitations of conventional joining methodologies. It facilitates the welding of diverse range of materials like metals, non-metals, polymers etc. Laser transmission welding is a technique employed for fabricating intricate shapes/contours in polymers with better precision compared to the other conventional processes. Nylon6, a synthetic semi-crystalline polymer is utilized as an engineering thermoplastic due to its high strength and temperature resistant properties. In the earlier researches, various welding techniques were employed for the fabrication of polymers and metals keeping the laser beam stagnant, and much emphasis was given only to temperature distribution along the different axes and limited attention was given to residual stress analysis. Therefore, in this research work, a three-dimensional time-dependent model using a moving laser beam is used to fabricate unreinforced Nylon6 specimens.

Keywords
laser transmission welding, simulation, through transmission laser welding, glass transition temperature, finite element method.

Introduction

In the early 1970s, innovative concepts resulted in the breakthrough of extensive usage of lasers in industries for machining, cutting, engraving and welding of sheets of metals and plastics. On the other hand, laser welding of polymers demonstrated its future prospects in the area of production in the starting phase of 1990s. But, due to high investment cost, the aforesaid process is not economically viable. Hence, assembly of thermoplastics by laser welding is going through prolonged experimental study during the last two decades, as many automotive and plastic engineers are not well acquainted with this technology. Laser welding of thermoplastics is comparatively new technology with respect to the conventional fusion techniques of plastics, such as ultrasonic, spin, stir, kinetic, electromagnetic, hot plate, hot-gas, hot-air and extrusion welding. Welding technology of plastics is influenced by the energy delivered to the area of the future joint (weld) in order to create melt-pool. After cooling and solidification of melt pool two separate plastic sheets join into one solid piece. The localized heat input in laser welding induces less thermal and residual stresses over small area compared to long-established techniques to generate weld of high quality. Moreover, plastics are the most important and fast growing materials for basic needs due to their characteristics, like portability, corrosion resistance and weather resistance. They are also durable and have wide applications in medical, textile, automobile and aerospace industries. Laser welding of plastics is emerging as a new alternative over conventional plastic fabricating technology due to flexibility of the process and better weld quality. The present work contributes to the advancement of a three dimensional thermo-mechanical model with process simulation in the context of through

transmission laser welding of polyamide plastics. The COMSOL Multiphysics software with an integral finite element code and finite element method is employed where moving laser beam is considered inorder to quantify the variation in temperature dependent properties on the nodes i.e. considered as the small element of the work-piece. The significant and basic boundary conditions are taken as constraints or conditions that are to be satisfied for carrying out the welding. Through transmission laser welding (TTLW) of lap joint of polyamide material i.e. Nylon6 sheets having physical and optical properties is carried out by simulation experiments. In this experiment, two distinct sheets of Nylon 6 are used, the upper part is crystalline that allows the radiation to pass through it, whereas the lower part is radiation absorbing. A stimulated laser beam is passed over the transparent polyamide material that overlaps the opaque polyamide material taking into account all the significant considerations along with physical properties of the materials that are temperature dependent. In the simulated three-dimensional model development, temperature varying material properties of polyamide are specified as input along with geometric details of the material model. Laser process parameters such as beam diameter, beam power and scanning speed are considered, and these input parameters are varied in levels and the corresponding results are noted. Those recorded effects of varying input parameters on the weld quality are studied through single and multi-objective optimization techniques to identify the optimum parametric conditions for thermo-mechanical analysis of Nylon6. The obtained optimum parametric conditions help in optimizing the fabrication of Nylon6 with desirable properties.

Review of past researches

In this highly competitive world, welding of different polymers with desired weld strength, melt penetration, residual stresses and width of heat affected zone is critical to attain long term sustainability and profitability for any modern day manufacturing organization. In the past, huge amount of work has been carried out to study the significance of different welding parameters such as beam diameter, scanning speed, laser power and clamp pressure on the above responses. Coelho [1] carried high-speed laser welding of thin plastic films and studied the impact of dimensions of laser beam spot on strength of the weld. Kurosaki [2] obtained high welding strength and excellent surface appearance without causing thermal damage to the surface as often suffered in conventional direct infrared radiation welding process applying heat transfer techniques of simultaneous radiation and conduction processes. Ilie et al. [3] estimated the weldability of a polymeric material couple with respect to their thermal and optical properties. Casalino and Ghorbel [4] investigated laser welding of thermoplastic polymers for keyhole by finite element simulation. Coelho [5] modelled high-speed laser lap welding of thermoplastic films and studied the influence of laser beam spot shape, dimensions and position relative to sample displacement. Amanat [6] determined the influence of laser intensity, scan speed, and material morphology on the lap-joint bond strength of poly-ether-ether-ketone joined using transmission laser welding. Kurosaki and Satoh [7] analyzed an innovative fiber laser welding method for engineering plastics assisted by a solid heat sink, transparent to the laser beam for preventing any thermal damage on the surface. Zak [8] presented a technique to obtain the distribution of the laser energy across the weld line through the information gathered from line width and power. Acherjee [9] established a correlation between the laser transmission welding parameters and output variables though a nonlinear model, developed by applying artificial neural network (ANN). Tu and Paleocrassas [10] examined whether crack could be first fused by laser welding to remove the high stress concentration at the crack front before applying the composite patch to further enhance its effectiveness. Cho [11] evaluated the effects of laser beam profile (Gaussian vs. measured), vapour shear stress, vapour heat source and sulphur content on the molten pool behaviour and shape of fusion zone. Devrient [12] studied characterization of the scattering behaviour of semi crystalline thermoplastics fibers on the calculated temperature fields and weld seam geometries. Han [13] conferred a study which proposed that the welding induced distortions are highly dependent on the geometry of the molten zone and the heat affected zone. Wippo et al. [14] presented a quasi-simultaneous laser transmission welding techniques with part adapted temperature fields and on-axis pyrometric-based temperature measurement method suitable for contour welding. Chaowen and Yong [15] ascertained the influence of flowing water on the temperature field and stress distributions of in-service welding of X70 steel pipeline. Devrient et al. [16] developed contour laser transmission welding with part-adapted temperature fields and experimentally investigated the process to obtain more precise technique which could measure temperature variation. Mamuschkin [17] studied different types of laser sources that could be used for welding of polymer by laser transmission welding. Reinl [18] studied laser welding of plastics using

diode laser which proved to be ideal tool due to fast power controllability and contactless temperature measurement to minimize thermal damage. Arif and Chung [19] proposed a method based on drop size information to predict the range of the joint gap that could be bridged effectively in alternating current-gas metal arc welding. Cho [20] conducted numerical simulation by FEM, finite differential method and volume of fluid method to understand arc welding, laser welding and laser-arc hybrid welding processes. Liu [21] observed a linear relationship between friction lap welding (FLW)parameters (R/v)0.5 and the thickness of melted nylon through a case study on aluminium alloy AA6061 and Monomer Casting Nylon6. Wang [22] determined that the molten pool depth to melt width ratio has a significant influence on the shear strength of the laser welded joint of polyethylene and polypropylene. Metais [23] characterized numerically and experimentally materials mixing during laser welding of steel and nickel. Simulation was carried out considering the fluid flow, heat and mass transfer. Tomashchuk et al. [24] studied the dynamics of keyhole in continuous and pulsed mode laser welding of two disimilar metal i.e., steel and Ti6Al4V. Finite element simulation study was carried to compare the discontinuity in the properties of two metals across the weld bead. Pagano [25] studied the possibility of laser transmission welding of aluminium to polyactide using pulsed laser beam of lower power. Tensile strength, weld width and weld defects were studied for evaluation of quality of joint and to quantify its strength. Millot [26] studied the deformation mechanism of Nylon 6 under tensile stretching. The study was carried out below and above of glass transition temperature. Kanigalpula [27] carried out the input-output modeling to optimise the spiking phenomenon in the electron beam welding of copper plates. Jina [28] developed mixed and non-linear regression equations to study the strength of the concrete It is evident from the review of past researches that only limited work has been carried out related to TTLW of various plastics. Moreover, in past, researchers had mostly studied the TTLW process, considering a constant spot diameter of laser beam. Therefore, the objective of the present work not only includes thermal analysis, but it also comprises analysis of residual stresses developed during welding. This proposed study also evaluates time varying responses with the moving laser beam. FEM is a powerful tool and is generally applied for simulation of laser welding processes including TTLW of plastics. It not only yields useful data, but also can help in the analysis of thermo-mechanical behavior during the process. It is evident from the past research that Taguchi L9 method and nonlinear regression equation has been implemented to carry out welding.

Thus, the present work employs a FEM for simulating through transmission laser welded lap joint of Nylon6.

Methodology

Numerical simulation for the welding process helps to predict the geometry of the joint, microstructure and other fabrication characteristics. Experimental based trial and error method is expensive and time consuming, therefore numerical analysis is partially adopted as a valid tool and is widely applied in the fabrication process. Laser welding is the joining process by the irradiation by photons. The current research work deals with TTLW of Nylon6. The three welding parameters are enlisted in Table 2 and nine lap joints of Nylon6 sheets are welded by simulation experiments as per Table 3. Each sample constitutes of two such pieces welded together. Laser beam is moved through mid-position of this overlapping and it is scanned over in the Y direction as indicated in Fig 1. Dimensions of each sample are 100 mm x 50 mm x 3 mm are shown in Fig 2. Origins of X, Y and Z for FEM and simulation are also indicated in Fig 1, which are X = 0 at one end (left end) of the opaque part, Y = 0 at the starting point of the laser beam scanning and Z = 0 at the interface of the two parts, i.e. positive (+) upward and negative (–) downward. For FEM, half of the overlapped portion comprising both the transparent (top) part and the opaque (bottom) part is taken into account. This portion is discretized by using three dimensional (3D) finite elements. Symmetric boundary conditions are considered for the simulation experiment. Here, symmetric conditions are assumed for both the halves in order to minimize the simulation time and obtain the desired results. The upper part is transparent the lower one is opaque that are sheets of Nylon6. The transparent sheet allows the laser beam to pass through it and the opaque one absorbs the laser beam falling on the experimental setup. As the laser beam is absorbed it results in melting of the opaque sheet and there is melting of the transparent sheet due conduction at the surface where the two sheets overlaps.

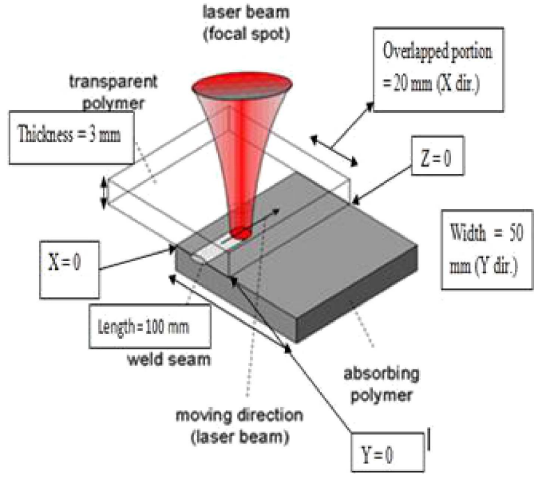

Fig. 1. Through transmission laser welding of plastics.

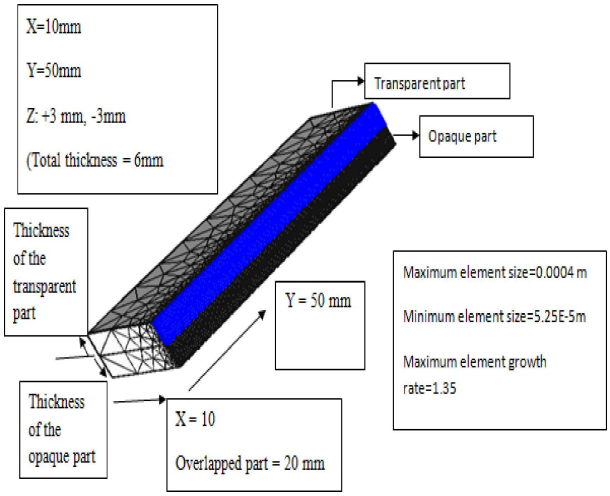

Fig. 2. Discretized region of the overlapped portion.

Thermo-mechanical analysis of a 3D time dependent model of lap joint being welded by a moving laser beam is performed in order to obtain results for the analysis of thermo-mechanical properties. Developed model is also utilized to handle the design of simulation experiments to be carried out at varied levels of input parameters. The model is based on FEM simulated in COMSOL Multiphysics where the physical phenomena like conduction, convection and radiation losses are considered. Temperature (T) dependent physical property is depicted in Table 1 viz. thermal conductivity (k). The emissivity of the material is temperature dependent. The relation of emissivity with temperature is given by Eq. (1)

$$\xi_\lambda = 0.365^*(\rho/\lambda)^{0.5} - 0.0667^*(\rho/\lambda) - 0.006^*(\rho/\lambda)^{1/3}, \quad (1)$$

where, ξ_λ is the emissivity of substrate, ρ is the substrate electrical resistivity in ohm-metre and λ is the wavelength of the laser beam in metres. Considering the various modes of heat transfer the different phases of heating and cooling of welding are modelled and the residual stress-strain behaviour is expressed by the application of multilinear isentropic hardening model that integrates the Von Mises yield criteria.

Table 1
Temperature depended properties of Nylon6.

T [K]	k [W/mK]
187	.287
244	.322
296	.332
300	.348
333	.346
405	.355
467	.358
490	.357
533	.147

Experiment setup is designed for the analysis by Taguchi's L9 orthogonal array. The three parameters considered for the above experiment are laser power (P), scanning speed (V) and laser beam diameter (D) have been varied over three levels as enlisted in Table 2.

Table 2
Process control parameters, their levels and their units.

No.	Parameters	Unit	Level 1	Level 2	Level 3
1	Power (P)	[W]	6	7	8
2	Scanning speed (V)	[mm/min]	300	350	400
3	Beam diameter (D)	[mm]	1.5	1.75	2

Graphs showing relations between the input parameters and the responses such as temperature melt width, depth of penetration and residual stresses in the specimen after welding are plotted using Origin 8 software. Optimized results are obtained using MINITAB software in order to complete the study successfully. Design matrix for the same is shown in Table 3.

Table 3
Design matrix of experiments using Taguchi's L9 orthogonal array design.

No.	Power (P) [W]	Scanning speed (V) [mm/min]	Beam diameter (D) [mm]
1	6	300	1.50
2	6	350	1.75
3	6	400	2.00
4	7	300	1.75
5	7	350	2.00
6	7	400	1.50
7	8	300	2.00
8	8	350	1.50
9	8	400	1.75

The responses obtained from the plots i.e. simulated results are maximum temperature (Tmax), weld width (WW), residual stresses, penetration depth (melt depth) in the transparent part (DT) and absorbing part (DA). Numerically simulated results are presented in Table 4. The developed model derives its eminence from the fact that it is applicable in probabilistic studies of a wide spectrum of research on TTLW problems of various geometrical and weld configuration. In order to develop the model one requires basic thermo-mechanical properties of the material. The prerequisites are geometrical dimensions, whereas laser parameters are considered as inputs.

Table 4
Simulated results of experiments for maximum temperature, weld width, penetration depth.

No.	Welding parameters			Simulated results	
	Power (P) [W]	Scanning speed (V) [mm/min]	Beam diameter (D) [mm]	Weld width (WW) [mm]	Total penetration depth PD (DA+DT) [mm]
1	6	300	1.50	0.360	0.300
2	6	350	1.75	0.130	0.420
3	6	400	2.00	0.340	0.202
4	7	300	1.75	0.210	0.328
5	7	350	2.00	0.400	0.310
6	7	400	1.50	0.490	0.360
7	8	300	2.00	0.500	0.301
8	8	350	1.50	0.503	0.390
9	8	400	1.75	0.510	0350

The basic idea of FEM is to make calculations at only limited number of points and then interpolate entire domain (surface or volume). Any continuous object has infinite degrees of freedom and therefore it is tedious job to calculate by conventional process. FEM reduces the degrees of freedom from infinite to finite with the help of discretization or meshing (nodes and elements). Mathematical operation of integration is applied inorder to obtain responses over the entire body. The smallest part of the surface or volume is named as element. Element considered for meshing the entire model is a 4 node tetrahedral element in the simulation experiments. The element has a 3D thermal conduction capability and applicable for a transient thermal analysis. Free convection and radiation losses from surfaces are considered as boundary conditions.

Specified convection and radiation surfaces acting over surface is given by the following equation:

$$\{q\}^T\{\eta\}^T = h(T_S - T_B) + \sigma\xi(T_S^4 - T_B^4), \qquad (2)$$

where $\{\eta\}$ is the unit outward normal vector, T is the overall temperature of the element, h is the convective heat transfer coefficient (W/m^{2}K), T_S is the surface temperature (K) of the model, T_B is bulk temperature (K) of the adjacent fluid, ξ is the material emissivity and σ is the Stefan Boltzmann constant (5.67×10^{-8} W/m^{2}K). A non-uniform mesh pattern is generated to minimize the simulation time. The region near the laser irradiation is fine meshed because the high heat flux is involved in this portion. In the other region coarser meshing is done. Mesh generated image of one-half of the overlapped part is shown in Fig. 3. Meshing is done in order to obtain approximate result.

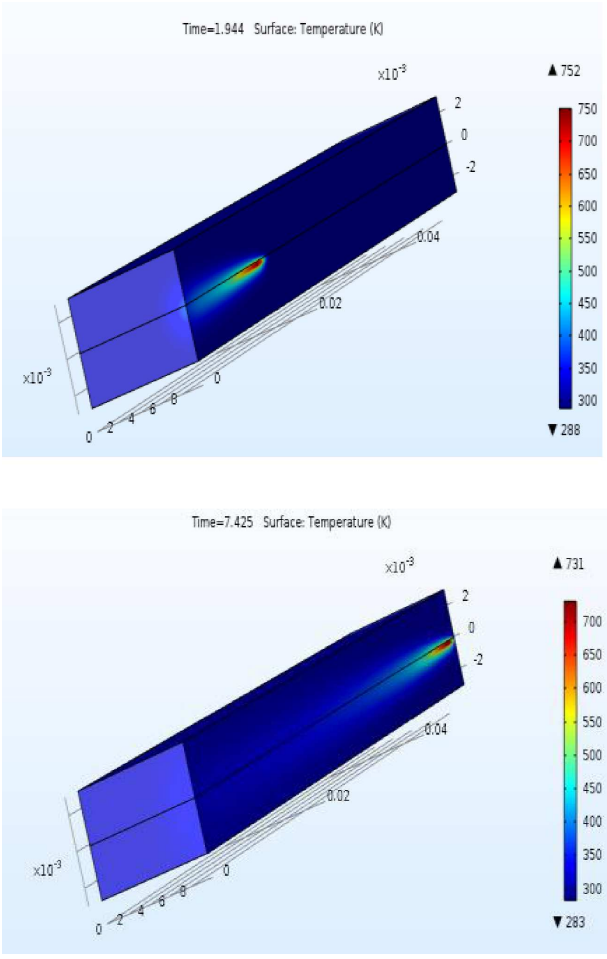

Fig. 3. Temperature distributions at weld interface and position of laser beam with respect to varying time.

Results

The objective of the present work is to categorize the effects of process parameters on maximum temperature,penetration depth and weld width in TTLW of Nylon6 by finite element analysis. The parameters like laser power, scanning speed and beam diameter have been varied over three levels to obtain different responses such as, melt penetration (penetra-

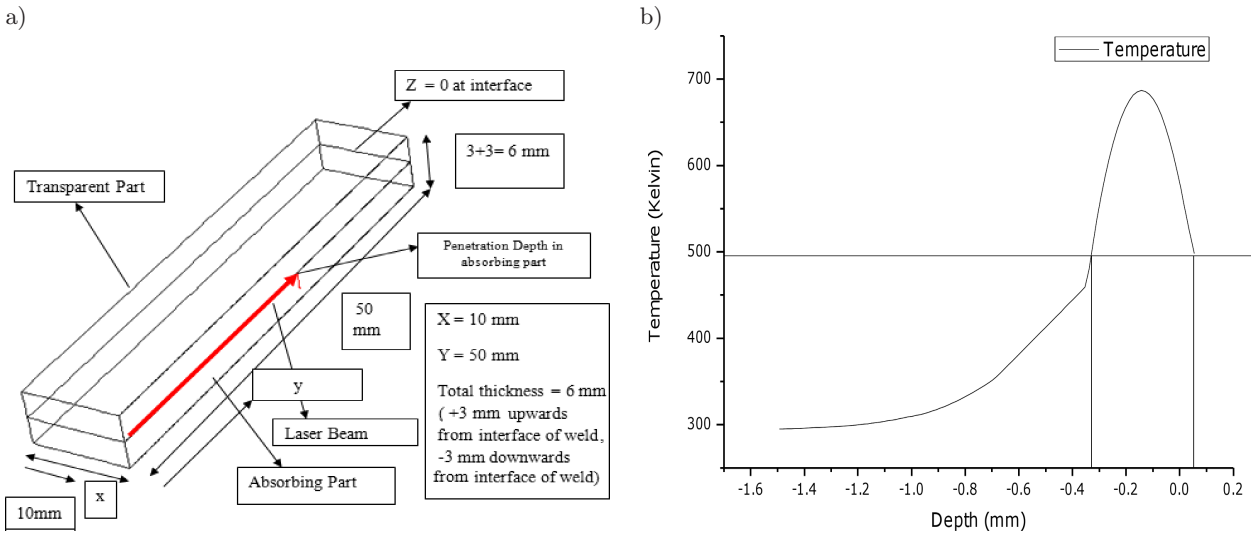

Fig. 4. The temperature distribution along with the penetration depth: a) distance or point where penetration is measured, b) graphical representation of penetration depth.

tion depth), weld width, maximum temperature and residual stress for each of the nine experiments. Figure 3 exhibits temperature distribution on the symmetry (Y-Z) plane of the lap joint that has been exposed to moving laser beam at different time intervals as follows:

(a) At $t = 1.94$ second when the laser beam is just at the beginning of interface,

(b) At $t = 7.42$ second when the laser beam is about to complete welding.

The temperature variations are recorded at the above time intervals. It is observed from the derived results that the maximum temperature reaches 686.66 K during welding. The glass transition temperature of Nylon6 is around 490 K. The Fig. 3 is in context of the experiment no. 6. In the referred experiment the laser power, scanning speed and beam diameter is taken as 7 W 400 V 1.5D respectively. Simulation has been done for all other combinations of the input parameters as per Table 3.

The temperature distribution along with the penetration depth is illustrated in Fig. 3 i.e. along the thickness (Z axis) of both the absorbing and the transparent parts for the condition of 7 W 400 V 1.5D. The maximum temperature reached in this case is 686.66 K. Melting at the interface and penetration depth in the transparent and opaque Nylon6 sheets occurs. The location of the point where penetration depth in transparent part DT and penetration depth in DA has been measured for experiment no. 6 that is illustrated in Fig. 4a at $Y = 28.75$ mm and the plot depicted in Fig 4b helps to find the penetration depth along specified co-ordinate at some explicit time. At this juncture, MS-Excel sheets assists to quantify the penetration depth in the absorbing part and in the transparent part are determined for the condition of experiment no. 6 during simulation. The product of scanning speed and time gives the specific location of Y axis at which the penetration depth is measured.

Simulation for temperature distribution at weld interface in reference to weld width is presented in Fig. 5. This is for the sample corresponding to experiment no. 6 (7 W 400 V 1.5D). The weld width is measured along X-Y plane, scanning between the co-ordinates ($X = 0$, $Y = 28.75$, $Z = 0$) mm at one point and with co-ordinates ($X = 10$, $Y = 28.75$, $Z = 0$) mm at other end. From Fig. 5b, weld width is determined, corresponding to the condition at which temperature reaches beyond the glass transition temperature. It can again be mentioned that WW here is the width of the weld seam from the center line of the laser beam to one side of the overlapped portion; i.e. it is almost half of the total width of weld seam.

The next stage of thermo-mechanical analysis comprises of determination of residual stress developed during TTLW of Nylon6, under varied levels of the input parameters. The types of residual stresses induced are residual tensile stress and residual compressive stress. After attaining a peak value compressive residual stress gradually decreases owing to softening of metal being heated. Compressive residual stress near the faying surfaces eventually reduces to zero as soon as melting starts and a reverse trend is observed during cooling stage of the welding. During cooling as metal starts to shrink, tensile residual stresses develop (only if shrinkage is not allowed either due to metallic continuity or constraint from job clamping) and their magnitude keeps on increasing

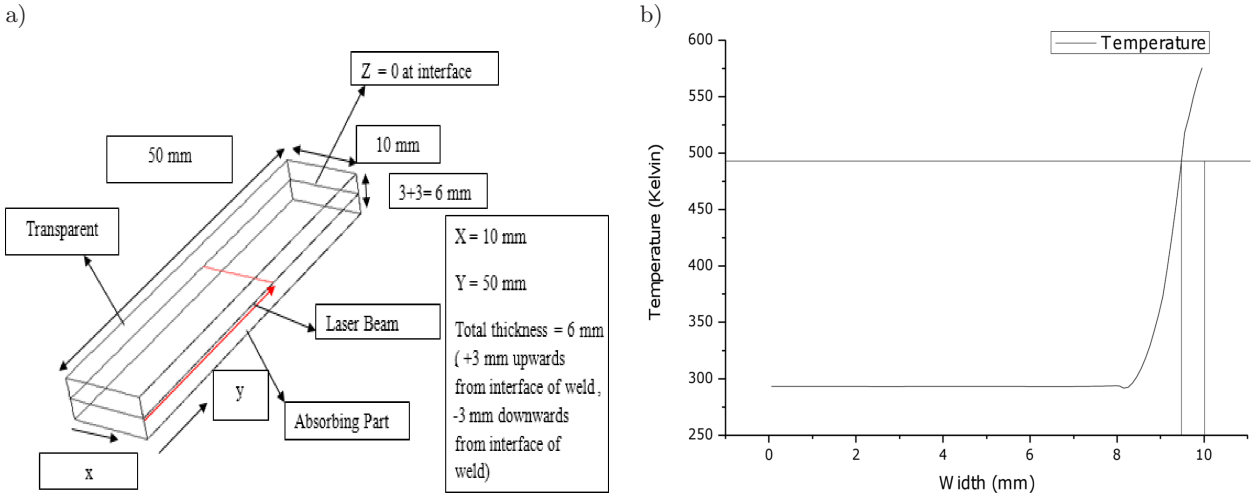

Fig. 5. The temperature distribution along the weld-width: a) location of the weld width measurement, b) graphical presentation of the weld width with the respect to temperature (K) and the width (mm).

until room temperature is attained. In general, greater is degree of constraint and elastic limit of melt higher will be the value of residual stresses. The residual stresses are analysed as they can lead to material failure or deformation. The residual stresses developed in three axes at different time can be determined while using FEM. However, in the present work more importance has been given to residual stress in the X direction, measured along different Y co-ordinates during total scanning time. The results obtained are listed Table 5. Residual tensile stress is taken into consideration as it is more harmful than residual compressive stress. Figure 6 illustrates the residual stress for experiment no. 1 with input parameters: (6 W, 300 V, 1.5D) Distribution of residual stress is depicted by Fig. 6. It is noticed that during time interval, $t = 0$ to 20 seconds, residual stresses

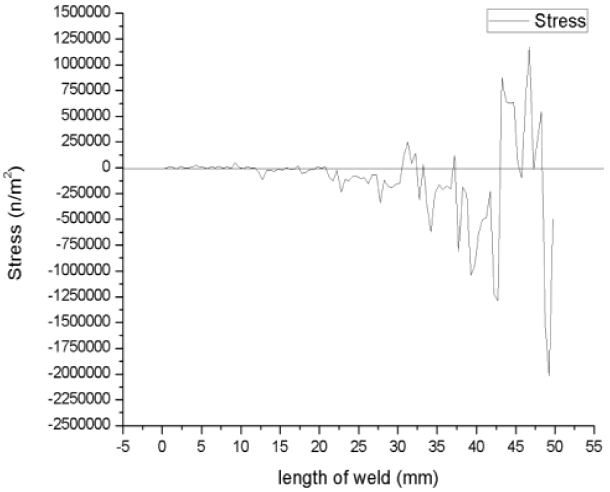

Fig. 6. Plot of residual stress in the X direction along scanned length.

Table 5
Simulated results of residual stress.

Experiment No.	Welding parameter			Stimulated results
	Power P [W]	Scanning speed V [mm/min]	Beam diameter D [mm]	Maximum residual stress (S) in X direction [N/M^2]
1	6	300	1.50	1172034
2	6	350	1.75	1487793
3	6	400	2.00	243912.2
4	7	300	1.75	1185487
5	7	350	2.00	792813.2
6	7	400	1.50	1016536
7	8	300	2.00	2982952
8	8	350	1.50	2398665
9	8	400	1.75	1194347

are built up in the job. The residual stresses are of both tensile and compressive natures. Tensile residual stress is more fatal as it results to cracks and failure of the material.

Results of the experiments conducted by finite element simulation have been exhibited. Results have been analyzed in this section for both single objective optimization and multi- objective optimization of through transmission laser welding of Nylon6. Taguchi's S/N ratio concept has been used for single objective optimization, for which the optimum parametric conditions are identified for minimization of weld width, maximization of penetration depth and for attenuation of the residual stresses in the welded parts, Grey relational analysis combined with Taguchi's methodology is used for minimization of

weld width, maximization of penetration depth and minimization of the residual stresses induced due to the temperature, simultaneously. Analysis of variance(ANOVA) helps to find the relative significance of weld parameters on the individual responses and as well as on the overall grey relational grade. Main effects plot and analysis of variance for penetration depth, weld width and residual stress. In order to identify the welding characteristics, the experimental data is analyzed and the observed data contained in Table 4 and Table 5 are used to determine main effects plots. MINITAB software is employed for this purpose and the means of the responses is obtained first. Then main effects plots are generated. ANOVA is also carried out. These steps are followed for all the responses i.e. penetration depth, weld width (half of the seam width) and residual stress (S).

Penetration depth (PD)

It is observed from Fig. 8 and Table 6 that penetration depth increases with the increase in power and tends to decrease with the increase in scanning speed and beam diameter. This phenomenon can be attributed to the development of more heat intensity with the rising in temperature value. In case of high scanning speed, the surface is heated for a small duration; therefore, less heat is absorbed by the welding surface, which results in low temperature. There is more time to heat the surface when the scanning speed is slow which results in consumption of more heat energy and thus increasing the temperature. When the beam diameter is small, the heat intensity is more as it falls on a smaller area, therefore rising the temperature. On the other hand, when the beam diameter is larger, the heat falls on larger surface reducing the beam intensity due to the distribution of heat, thus resulting in low temperature. Results of ANOVA for penetration depth are listed in Table 7.

Table 6
The response values for mean of penetration depth.

Level	Power [W]	Scanning speed [mm/min]	Beam diameter [mm]
1	0.3073	0.3097	0.3500
2	0.3321	0.3733	0.3660
3	0.3470	0.3040	0.2710
Delta	0.0397	0.0693	0.0950
Rank	3	2	1

The terms used in all ANNOVA tables are standard ones, with their usual meanings. As far as significance of all the factors is concerned, ANNOVA table indicates that none of the factors are significant at 95% confidence level, as 'P' values corresponding to each input parameter are more than 0.05. However, considering relative importance, beam diameter influences penetration depth most significantly, followed by scanning speed and then power and in case weld width of power influences most significantly, followed by diameter and then comes scanning speed.

Table 7
Analysis of variation for means of penetration depth.

Source	DF	Seq SS	Adj SS	Adj MS	F	P	Percentage contribution
Power	2	0.002	0.002	0.001	0.52	0.659	7.60%
Scanning speed	2	0.008	0.008	0.004	1.90	0.345	28.23%
Beam diameter	2	0.015	0.015	0.007	3.31	0.232	49.24%
Residual error	2	0.004	0.004	0.002			14.86%
Total	8	0.031		$R-sq = 85.14\%$	$R-sq(\text{adj}) = 70.28\%$		

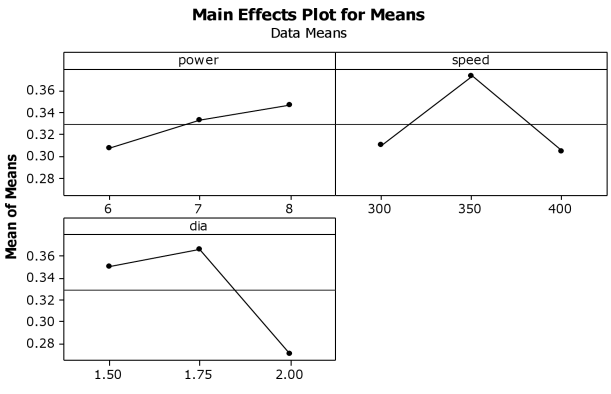

Fig. 7. Main effects plot for mean of penetration depth.

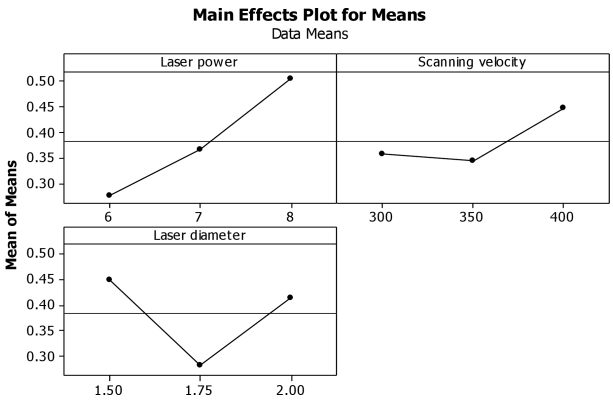

Fig. 8. Main effects plot for mean of weld width.

Weld width (WW)

It is observed from Fig. 9 that weld width increases tends to decrease with the increase in scanning speed, though not consistently. This phenomenon can be attributed to the development of more heat intensity with increase in temperature. In case of high scanning speed, the surface is heated for a small duration; therefore, less heat is absorbed by the welding surface, which results in low temperature. There is more time to heat the surface when the scanning speed is slow which results in consumption of more heat energy and thus increasing the temperature. Increase in scanning speed has roughly resulted in increase in weld width. Insufficient time at high speed probably retards penetration which tends to increase weld width to some extent. When the beam diameter is small, the heat intensity is less as it falls on a smaller area, thus enhancing the temperature but heat is concentrated over small area and thus small weld width is expected to be obtained. On the other hand, when the beam diameter is larger, the heat falls on larger surface reducing the beam intensity due to the distribution of heat, thus increasing the weld width. But the trends shown in shown in Fig. 9 are not found to be consistent with the above logic. The response data for means of weld width and ANOVA table for weld width are obtained as shown in Table 8 and Table 9 respectively.

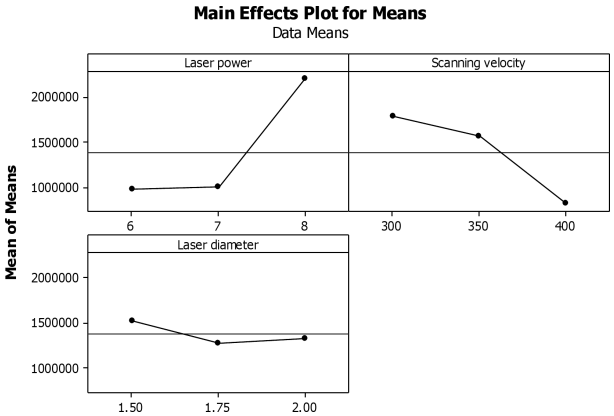

Fig. 9. The main effects plot for mean for residual stress.

Table 8
The response values for mean of weld width.

Level	Power [W]	Scanning speed [mm/min]	Beam diameter [mm]
1	0.2767	0.3577	0.4500
2	0.3667	0.3433	0.2833
3	0.5043	0.4467	0.4143
Delta	0.2277	0.1033	0.1667
Rank	1	3	2

ANOVA Table 9 indicates that none of the factors is significant at 95% confidence level, as 'P' value corresponding to each input parameter is more than 0.05. However, considering relative importance, power influences weld width most significantly, followed by beam diameter and then scanning speed.

The results of nine simulation experiments are listed in Table 5 that are used to obtain mean response data of residual stresses tabulated in Table 10 and Fig. 10 depicts the Main effects plot for residual stress. The results of ANOVA are listed in Table 11. It is evident from Fig. 10 that the residual stress in the material increases with the increase in power and decreases with the increase in scanning speed beam diameter. The increase in residual stress is attributed to more deformation of material with respect to power increment. Lower level of scanning speed and small beam diameter will result in less deformation of work-piece. However, this explanation may get refined through more experiments and analyses.

Table 10
Response data for means of residual stress.

Level	Power [W]	Scanning speed [mm/min]	Beam diameter [mm]
1	967913	1780158	1529078
2	998279	1559757	1289209
3	2191988	818265	1339892
Delta	1224075	961893	239869
Rank	1	2	3

Table 9
Analysis of variation for means of weld width.

Source	DF	Seq SS	Adj SS	Adj MS	F	P	Percentage contribution
Power	2	0.078	0.078	0.039	9.42	0.096	51.80%
Scanning speed	2	0.018	0.018	0.009	2.25	0.308	12.34%
Beam diameter	2	0.046	0.046	0.023	5.52	0.153	30.34
Residual error	2	0.008	0.008	0.004			5.52%
Total	8	0.152		$R-sq = 94.48$	$R-sq(\text{adj}) = 88.96\%$		

Table 11
Analysis of variation for means for residual stress.

Source	DF	Seq SS	Adj SS	Adj MS	F	P	Percentage contribution
Power	2	2.92×10^{12}	2.92×10^{12}	1.46×10^{12}	3.05	0.247	53.09%
Scanning speed	2	1.52×10^{12}	1.52×10^{12}	7.62×10^{12}	1.59	0.386	27.67%
Beam diameter	2	9.59×10^{11}	9.59×10^{11}	4.79×10^{11}	0.10	0.909	17.43%
Residual error	2	9.57×10^{10}	9.57×10^{11}	4.78×10^{11}			1.81%
Total	8	5.50×10^{12}		$R - sq = 98.19\%$	$R - sq(\text{adj}) = 89.48\%$		

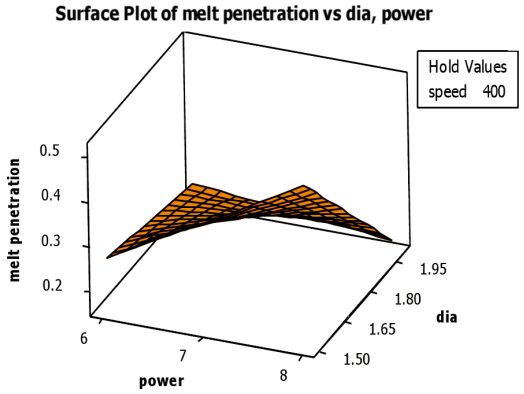

Fig. 10. Response surface showing combined effect of power and beam diameter on penetration depth at scanning speed = 400 mm/min.

It can be noticed from the Fig. 9 that residual stress in the material increases with the increase in power and decreases with the increase in scanning speed and beam diameter. The increase in residual stress is attributed to more deformation of material with respect to power increment. On the other hand, higher scanning speed with small beam diameter means that there would be less deformation of work-piece. Therefore, residual stress decreases with increase in scanning speed and decrease of beam diameter.

Table 11 indicates that no parameter has significant role in influencing residual stress at 95% confidence level. 'P' value for each of the factors is less than 0.05. However, percentage contribution of power is found to be largest; followed by scanning speed and least is of the beam diameter.

Mathematical modelling and response surface plots

Response surface methodology is adopted to corelate the input parameters P, V and D with each response (PD, WW and S) separately. The form of equation considered is the type shown in Eq. (3)

$$\begin{aligned} Y = \beta 0 + \beta 1(P) + \beta 2(V) + \beta 3(D) + \beta 4(PV) \\ + \beta 5(VD) + \beta 6(PD). \end{aligned} \tag{3}$$

Using MINITAB software and utilizing the simulated data in Table 4 and Table 5, the coefficients β_0, β_1, etc. are determined and response equations are developed [27, 28]. The confidence area for the developed regression equations is 95%. These are shown in Eqs. (4)–(6)

$$\begin{aligned} PD = -3.74 - 0.089P + 0.0026V + 4.88D \\ + 0.00162P^*V - 0.291P^*D - .00810V^*D, \end{aligned} \tag{4}$$

$$\begin{aligned} WW = 7.74 - 0.073P + 0.0018V - 9.4D \\ - 0.00280P^*V + 0.708P^*D + 0.01169V^*D, \end{aligned} \tag{5}$$

$$\begin{aligned} S = -10430542 + 2787904P + 68913V \\ - 11067271D - 11869P^*V \\ + 1145571P^*D + 4237V^*D, \end{aligned} \tag{6}$$

where PD = penetration depth, WW = weld width and S is the residual stress. The range of the levels of the parameters used in the study, the above models can be used to predict or estimate the response values at varied or given combinations of the input parameters.

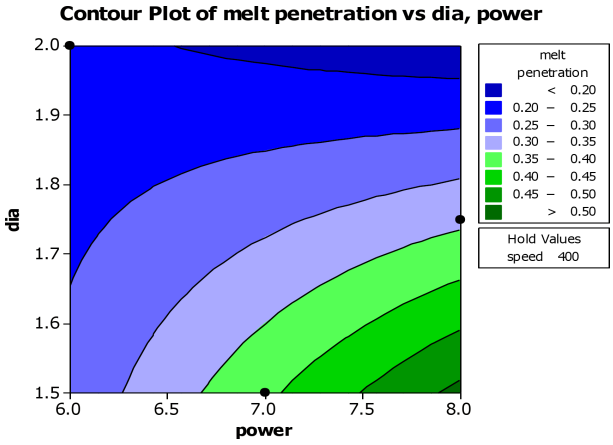

Fig. 11. Contour plots showing combined effect of power and beam diameter on penetration depth at scanning speed = 400 mm/min.

Parametric condition for grey relational grade

It is observed that the parametric conditions for maximum penetration depth are: P3 V2 D2 (i.e.

Power = 8 W, scanning speed = 350 mm/min and beam diameter = 1.75 mm). This is based on the level of each factor at which S/N ratio value is maximum. The optimum condition for weld width is P1 V2 D2 (i.e. Power = 6 W, scanning speed = 350 mm/min and beam diameter = 1.75 mm). For minimization of residual stress, the best condition is P1 V3 D3 (i.e. Power = 6 W, scanning speed = 400 mm/min and beam diameter = 2 mm). This is finalised corresponding to the levels of the factors at which S/N ratio values are maximum.

Grey relational grades

Now a weighing method is used to integrate the grey relational coefficient of each experiment into the grey relational grade. The overall assessment of the multiply quality characteristics is based on the grey relational grade which is given by Eq. (7)

$$Y_j = \frac{1}{m}\sum_{i=1}^{m} w_i \xi_{ij}, \tag{7}$$

where Y is the grey relational grade for the j-th experiment, w_i is the weighting factor for the i-th response and m is the total number of response. In calculating the grey relational grade, the weighting ratio for all the responses is set as 1:1, i.e., each characteristic has equal importance or relative weighting. The evaluated values of grey relational grades are depicted in the Table 14. The higher the value of grey relational grade, better is the desired response. S/N ratios of grey relational grade have been calculated by MINITAB and demonstrated in Table 15, where the value of delta is higher in case of power. Therefore, power has the more impact on the overall grey relational grade. Large value of grey relational grade is the objective, always. ANOVA for grey relational grade is shown in Table 16. The impact of the input parameters on the overall multi-objective output response (ANOVA) is applied. ANOVA is carried out by comparing the F-test value of the parameter with the standard F table value (F0.05) at 5% significance and 95% confidence level. If P-values in the table are less than 0.05 than the corresponding variables are considered statistically significant.

In Table 16, the P values for power, scanning speed and beam diameter all are greater than 0.05 which means that these three parameters do not have significant effect on the grey relational grade at 95% confidence level. However, it is observed from this table that relatively, it is the factor P (Power) which influences most, the overall objective (grey relational grade).

Table 12
Normalized values of the responses.

Experiment No.	Penetration depth	Weld width	Residual stress
1	0.550459	0.605263	0.338849
2	0	0	0.45413
3	1	0.552632	
4	0.422018	0.210526	0.343761
5	0.504587	0.710526	0.200399
6	0.275229	0.947368	0.282078
7	0.545872	0.981579	1
8	0.137615	0.973684	0.786682
9	0.321101	1	0.346996

Table 13
Values of grey relational coefficients corresponding to 9 experiments.

Experiment No.	$T_{\max}$	Weld width	Penetration depth
1	0.475983	0.452381	0.596055
2	1	1	0.524037
3	0.333333	0.475	1
4	0542289	0.703704	0.592585
5	0.497717	0.413043	0.713879
6	0.64497	0.345455	0.639322
7	0.47807	0.337478	0.333333
8	0784173	0.339286	0.388596
9	0.608939	0.333333	0.590322

Table 14
Calculated values of grey relational grade.

Experiment No.	Grey relational grade
1	0.508139
2	0.841346
3	0.602778
4	0.612859
5	0.541546
6	0.543249
7	0.38296
8	0.504018
9	0.510865

Table 15
Response table for S/N Ratio of grey relational grade.

Level	Power [W]	Scanning speed [mm/min]	Beam diameter [mm]
1	−3.926	−6.157	−5.710
2	−4.960	−4.260	−3.862
3	−6.707	−5.177	−6.020
Delta	2.781	1.897	2.158
Rank	1	3	2

Table 16
Analysis of variance for grey relational grade.

Source	DF	SEQ SS	ADJ SS	ADJ MS	F	P
Power	2	0.051	0.051	0.025	6.56	0.132
Scanning speed	2	0.024	0.024	0.012	3.16	0.240
Diameter	2	0.040	0.040	0.020	5.11	0.164
Residual error	2	0.007	0.007	0.003		
Total	8	0.123				

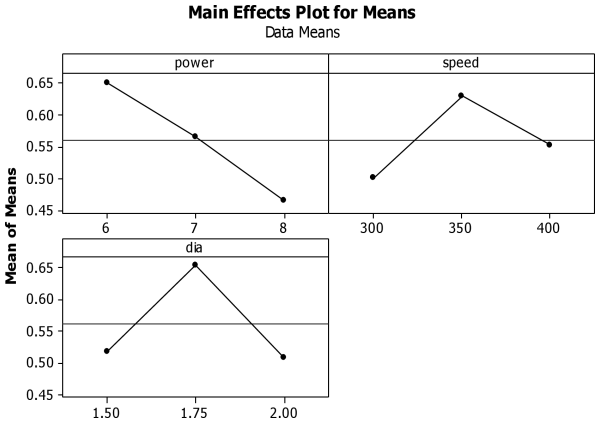

Fig. 12. Main effects plot for means for grey relational grade.

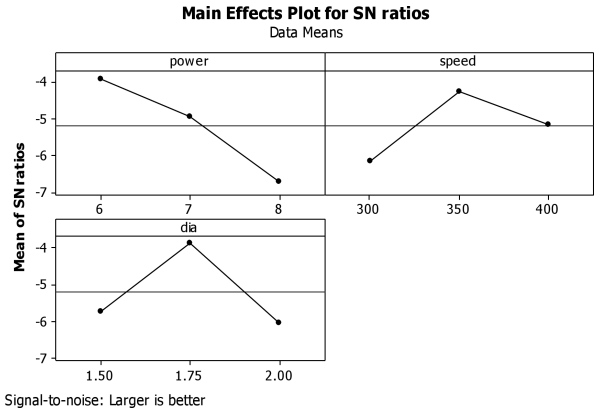

Fig. 13. Main effects plot for S/N ratios for grey relational grade.

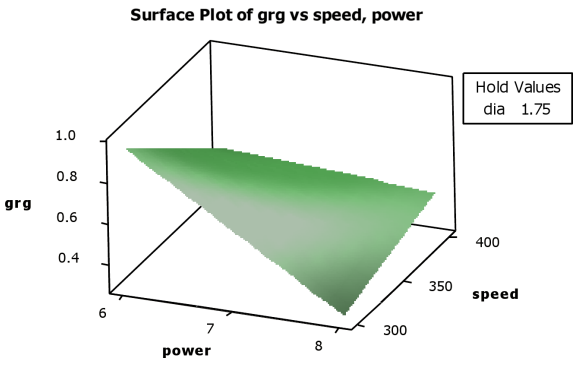

Fig. 14. Response surface showing combined effect of power and scanning speed on grey relational grade at beam diameter = 1.75 m.

Mean effects plot for grey relational grade and mean effects plot for S/N ratios is shown in Fig. 13 and Fig. 14 respectively. It is examined that for multi-response optimization, the optimum parametric configuration is power = 6 W, scanning velocity = 350 mm/min and beam diameter = 1.75 mm (P1 V2 D2), corresponding to the levels of the highest S/N ratio values of grey relational grades of these parameters.

Confirmatory test

Confirmatory experiment, through simulation, is made at optimum condition i.e., power (P1), scanning speed (V2) and beam diameter (D2) to validate the proposed methodology. It is actually the repetition of experiment no-2 It is observed that the optimized parametric combination produced penetration depth (PD) = 0.42 mm, maximum temperature = 647.28 K, weld width = 0.13 mm and residual stress = 1487793 N/m^2. These responses are satisfactory. The calculations were done to have convergence in the numerical formulation.

Conclusions

- In this research work, the effects of laser power, scanning speed and laser beam diameter on the weld width, melt penetration and residual stress have been studied and analyzed. Mathematical modelling is performed and the relationship between weld width, melt penetration, residual stress and process parameters has been developed.
- The developed model is employed to generate contour plots and response surface plots which can predict the responses adequately within the limits of welding parameters used. Response surface plots may be used to predict the response value at some given combination of any two parameters, while the third parameter being held at a constant level.
- It can be elicited from the derived results that laser power and laser beam radius has a strong interaction effect on seam width. These parameters control the heat input to the weld zone, and

thus, the quality of the weld. Besides, increasing laser power increases the weld seam width whereas, increasing laser beam radius increases the weld seam width.

- It is noticed that the optimum parametric condition for maximum melt penetration, minimum weld seam and minimum residual stress are 8 W 350 V 1.75 D, 6 W 350 V 1.75 D and 6 W 400 V 2 D respectively.
- In future, different combinations of transparent and coloured plastics can be considered for the study to predict and optimize the process parameters. Laser welding of transparent to coloured plastics is an interesting field of research.
- The perspective study can be helpful in modelling conduction and keyhole modes of laser welding for metals, alloys and non-metals such as plastics in automobile sector, structural materials used for erection of power plants and chemical factories to reduce the cost.
- Finite element analysis results in decreasing of the number of actual experiments that is required to be performed and thus, results in proper utilisation of resources.

References

[1] Coelho J., Abreu M., Pires M., *High-speed laser welding of plastic films*, Optics and Lasers in Engineering, 34, 385–395, 2000.

[2] Kurosaki Y., *Radiative heat transfer in plastic welding process*, Journal of Quantitative Spectroscopy and Radiative Transfer, 93, 25–41, 2005/06/15, 2005.

[3] Ilie M., Kneip J.-C., Matteï S., Nichici A., Roze C., Girasole T., *Through-transmission laser welding of polymers–temperature field modeling and infrared investigation*, Infrared Physics & Technology, 51, 73–79, 2007.

[4] Casalino G., Ghorbel E., *Numerical model of CO 2 laser welding of thermoplastic polymers*, Journal of Materials Processing Technology, 207, 63–71, 2008.

[5] Coelho J.M., Abreu M.A., Rodrigues F.C., *Modelling the spot shape influence on high-speed transmission lap welding of thermoplastics films*, Optics and Lasers in Engineering, 46, 55–61, 2008.

[6] Amanat N., Chaminade C., Grace J., McKenzie D.R., James N.L., *Transmission laser welding of amorphous and semi-crystalline poly-ether–ether–ketone for applications in the medical device industry*, Materials & Design, 31, 4823–4830, 2010.

[7] Kurosaki Y., Satoh K., *A fiber laser welding of plastics assisted by transparent solid heat sink to prevent the surface thermal damages*, Physics Procedia, 5, 173–181, 2010.

[8] Zak G., Mayboudi L., Chen M. , Bates P.J., Birk M., *Weld line transverse energy density distribution measurement in laser transmission welding of thermoplastics*, Journal of Materials Processing Technology, 210, 24–31, 2010.

[9] Acherjee B., Mondal S., Tudu B., Misra D., *Application of artificial neural network for predicting weld quality in laser transmission welding of thermoplastics*, Applied Soft Computing, 11, 2548–2555, 2011.

[10] Tu J., Paleocrassas A., *Fatigue crack fusion in thin-sheet aluminum alloys AA7075-T6 using low-speed fiber laser welding*, Journal of Materials Processing Technology, 211, 95–102, 2011.

[11] Cho W.-I., Na S.-J., Thomy C., Vollertsen F., *Numerical simulation of molten pool dynamics in high power disk laser welding*, Journal of Materials Processing Technology, 212, 262–275, 2012.

[12] Devrient M., Da X., Frick T., Schmidt M., *Experimental and simulative investigation of laser transmission welding under consideration of scattering*, Physics Procedia, 39, 117–127, 2012.

[13] Han Q., Kim D., Kim D., LeeH., Kim N., *Laser pulsed welding in thin sheets of Zircaloy-4*, Journal of Materials Processing Technology, 212, 1116–1122, 2012.

[14] Wippo V., Devrient M., Kern M., Jaeschke P., Frick T., Stute U., Schmidt M., Haferkamp H., *Evaluation of a pyrometric-based temperature measuring process for the laser transmission welding*, Physics Procedia, 39, 128–136, 2012.

[15] Li C., Wang Y., *Three-dimensional finite element analysis of temperature and stress distributions for in-service welding process*, Materials & Design, 52, 1052–1057, 2013.

[16] Devrient M., Kern M., Jaeschke P., Stute U., Haferkamp H., Schmidt M., *Experimental investigation of laser transmission welding of thermoplastics with part-adapted temperature fields*, Physics Procedia, 41, 59–69, 2013.

[17] Mamuschkin V., Roesner A., Aden M., *Laser transmission welding of white thermoplastics with adapted wavelengths*, Physics Procedia, 41, 172–179, 2013.

[18] Reinl S., *Diode lasers used in plastic welding and selective laser soldering – applications and products*, Physics Procedia, 41, 234–240, 2013.

[19] Arif N., Chung H., *Alternating current-gas metal arc welding for application to thin sheets*, Journal of Materials Processing Technology, 214, 1828–1837, 2014.

[20] Cho D.-W., Cho W.-I., Na S.-J., *Modeling and simulation of arc: laser and hybrid welding process*, Journal of Manufacturing Processes, 16, 26–55, 2014.

[21] Liu F., Liao J., Nakata K., *Joining of metal to plastic using friction lap welding*, Materials & Design (1980–2015), 54, 236–244, 2014.

[22] Wang X., Chen H., Liu H., *Investigation of the relationships of process parameters, molten pool geometry and shear strength in laser transmission welding of polyethylene terephthalate and polypropylene*, Materials & Design, 55, 343–352, 2014.

[23] Metais A., Mattei S., Tomashchuk I., Gaied S., *Modelling of Transport Phenomena in Laser Welding of Steels*, Proceedings of the COMSOL Conference, pp. 1–7, 2015

[24] Tomashchuk I., Bendaoud I., Sallamand P., Cicala E., Lafaye S., Almuneau M., *Multiphysical modelling of keyhole formation during dissimilar laser welding*, Proceedings of the COMSOL Conference, pp. 1–7, 2016.

[25] Pagano N., Campana G., Fiorina M., Morelli R., *Laser transmission welding of polylactide to aluminium thin films for applications in the food-packaging industry*, Optics & Laser Technology, 91, 80–84, 2017.

[26] Millot C., *Multi-scale characterization of deformation mechanisms of bulk polyamide 6 under tensile stretching below and above the glass transition*, Doctor of Philosophy's Thesis, National Institute of Applied Sciences of Lyon, https://tel.archives-ouvertes.fr/tel-01207840/ (accessed 29th May 2018).

[27] Kanigalpula P.-K.-C., Jaypuria S., Pratihar D.-K., Jha M.-N., *Experimental investigations, input-output modeling, and optimization of spiking phenomenon in electron beam welding of ETP copper plates*, Measurement, 129, 302–318, 2018.

[28] Jina R., Chen Q., Soboyejo A.-B.-O., *Non-linear and mixed regression models in predicting sustainable concrete strength*, Construction and Building Materials, 170, 142–152, 2018.